

Acylation of phenol on solid acids: Study of the deactivation mechanism

C.L. Padró, C.R. Apesteguía*

Catalysis Science and Engineering Research Group (GICIC), Instituto de Investigaciones en Catálisis y Petroquímica, INCAPE (UNL-CONICET), Santiago del Estero 2654, 3000 Santa Fe, Argentina

Available online 22 August 2005

Abstract

The deactivation mechanism of the gas-phase synthesis of *o*-hydroxyacetophenone (*o*-HAP) via acylation of phenol with acetic acid was studied on Al-MCM-41 and zeolites HY, HBeta and HZSM-5. The *o*-HAP yield remained constant with time-on-stream on HZSM-5 but drastically decreased on the other samples because of coke formation. The origin and nature of coke precursor species were studied by employing as reactants, the key reaction intermediates and products involved in the phenol acylation reaction network. It was found that coke precursors are formed from consecutive condensation reactions and not from any ketene formation by phenyl acetate decomposition. Specifically, it is proposed that *o*-acetoxyacetophenone (*o*-AXAP), which is formed by reaction between *o*-HAP and acetic acid, is the key intermediate specie responsible for the formation of carbonaceous deposits and consequently, for the activity decay observed on Al-MCM-41, HY and HBeta samples. The narrow pore size structure of zeolite HZSM-5 would hinder the formation of bulky *o*-AXAP, thereby, decreasing drastically the formation of coke.

© 2005 Elsevier B.V. All rights reserved.

Keywords: Catalyst deactivation; Acylation reactions; Solid acids; *o*-Hydroxyacetophenone synthesis

1. Introduction

Hydroxyacetophenones are useful intermediate compounds for the synthesis of important pharmaceuticals. In particular, *para*-hydroxyacetophenone (*p*-HAP) is widely used for the synthesis of paracetamol and *ortho*-hydroxyacetophenone (*o*-HAP) is a key intermediate for producing 4-hydroxycoumarin and warfarin, which are both, used as anticoagulant drugs [1,2]. In the classical commercial process, *p*-HAP is obtained via the Fries rearrangement of phenyl acetate in a liquid-phase process involving the use of homogeneous catalysts, such as AlCl₃, TiCl₄, FeCl₃ and HF, which pose problems of high toxicity, corrosion and spent acid disposal [3]. In an attempt to develop a suitable and environmentally benign process for producing *p*-HAP, strong solid acids, such as ion exchange resins, zeolites,

Nafion and heteropoly acids have been tested in liquid-phase for the Fries rearrangement of phenyl acetate. However, solid acids form significant amounts of phenol together with *p*-HAP and are in general rapidly deactivated [4–7]. On the other hand, the vapor-phase Fries rearrangement of phenyl acetate on solid acids produces mainly *o*-HAP, but formation of phenolic byproducts is significant and catalysts are deactivated because of coke formation [8,9].

Hydroxyacetophenones may be also obtained by the acylation of phenol in liquid- or gas-phases by employing different acylating agents. In liquid-phase, the reaction produces mainly *p*-HAP using either Friedel–Crafts or solid acid catalysts, but the process is hampered because of environmental constraints and catalyst activity decay [10–12]. In gas-phase, the phenol acylation on solid acids forms predominantly *o*-HAP, giving *o*-HAP/*p*-HAP molar ratios higher than 80 [13,14]. However, the reported experimental *o*-HAP yields are still moderate, particularly because of significant formation of phenyl acetate [15,16]; moreover, the catalyst activity decline on stream is often significant.

* Corresponding author. Tel.: +54 342 4555279; fax: +54 342 4531068.
E-mail address: capesteg@fiqus.unl.edu.ar (C.R. Apesteguía).
URL: <http://www.ceride.gov.ar/gicic>

From the above analysis of the literature, it is immediately inferred that the potential use of solid acids for obtaining hydroxyacetophenones in gas- or liquid-phases via either phenol acylation or phenyl acetate rearrangement reactions is limited because of the rapid activity decay. The development of more stable catalysts is therefore required to efficiently promote the synthesis of hydroxyacetophenones. However, very few studies have specifically focused on catalyst deactivation [7,17] and our understanding of the deactivation mechanism under reaction conditions is lacking. Taking this into account, we decided to perform a detailed study of the deactivation of solid acids during the gas-phase synthesis of *o*-HAP from the acylation of phenol with acetic acid. In a previous paper [18], we studied the gas-phase acylation of phenol with acetic acid over different solid acids with the objective of establishing the exact requirements of surface acid site density and strength to promote the *o*-HAP synthesis. Specifically, we employed solid acids containing only either strong Brönsted acid sites, such as HPA/C or moderate Lewis acid sites, such as zeolite NaY; catalysts containing both Lewis and Brönsted acid sites of either strong (zeolite HZSM-5) or moderate ($\text{SiO}_2\text{-Al}_2\text{O}_3$) strength were also used. We observed [18] that the *o*-HAP formation rate decreased on stream on all the solid acids excepting on zeolite HZSM-5. In basis of this observation, we decided to extent our studies focusing specifically on catalyst activity decay. In this paper, we studied the gas-phase synthesis of *o*-HAP from the acylation of phenol with acetic acid on Al-MCM-41 and zeolites HY, HBeta and HZSM-5. The objectives were two-fold: (i) to gain insight on the catalyst deactivation mechanism and (ii) to ascertain the causes for the superior stability of zeolite HZSM-5 on stream.

2. Experimental

Zeolite HY was prepared by triple ion exchange of a commercial NaY zeolite (UOP-Y 54) with ammonium acetate (Sigma, 99%) at 298 K and subsequent calcination in air. The H forms of zeolites, ZSM5 (Zeocat Pentasil PZ-2/54) and Beta (Zeocat PB), were obtained following the same procedure used for HY. Mesoporous Al-MCM-41 was synthesized according to Edler and White [19]. Sodium silicate solution (14% NaOH and 27% SiO_2 , Aldrich), cetyltrimethylammonium bromide (Aldrich), aluminum isopropoxide (Aldrich) and deionized water were used as the reagents. The composition of the synthesis gel was $7\text{SiO}_2\text{-}x\text{Al}_2\text{O}_3\text{-}2.7\text{Na}_2\text{O}\text{-}3.7\text{CTMABr}\cdot 1000\text{H}_2\text{O}$. The pH was adjusted to 10 using a 1 M H_2SO_4 solution, then the gel was transferred to a Teflon lined stainless-steel autoclave and heated to 373 K in an oven for 96 h. After crystallization, the solid was washed with deionized water, dried at 373 K and finally, calcined at 773 K for 4 h.

The crystalline structure of the samples was determined by X-ray diffraction (XRD) using a Shimadzu XD-D1

diffractometer and Ni-filtered Cu K α radiation. BET surface areas (S_g), mean pore diameter (\bar{d}_p) and pore size distribution were measured by N_2 physisorption at its boiling point in a Quantochrome Corporation NOVA-1000 sorptometer. Elemental compositions were measured by atomic absorption spectroscopy (AAS).

Acid site densities were determined by temperature-programmed desorption (TPD) of NH_3 preadsorbed at 373 K. Samples (200 mg) were treated in He (60 cm^3/min) at 773 K for 2 h and then exposed to a 1% NH_3/He stream for 40 min at 373 K. Weakly adsorbed NH_3 was removed by flowing He at 373 K during 2 h. Temperature was then increased at 10 K/min and the NH_3 concentration in the effluent was measured by mass spectrometry (MS) in a Baltzers Omnistar unit.

The nature of surface acid sites was determined by Fourier transform infrared spectroscopy (FTIR) by using pyridine as probe molecule and a Shimadzu FTIR-8101M spectrophotometer. Sample wafers were formed by pressing 20–40 mg of the catalyst at 5 tons/ cm^2 and transferred to a sample holder made of quartz. An inverted T-shaped Pyrex cell containing the sample pellet was used. All the samples were initially outgassed at 723 K for 4 h and then a background spectrum was recorded after cooling the sample at room temperature. Data were obtained after admission of pyridine, adsorption at room temperature and evacuation at 423 K. Spectra were always recorded at room temperature.

Coke formed on the catalysts during reaction was measured by temperature-programmed oxidation (TPO). Samples (50 mg) were heated in a 3% O_2/N_2 stream at 10 K/min from room temperature to 1073 K. The evolved CO_2 was converted to methane by means of a methanation catalyst (Ni/kieselghur) operating at 673 K and monitored using a flame ionization detector.

The gas-phase acylation of phenol (Merck, >99%) with acetic acid (Merck, 99.5%) was carried out in a fixed bed, continuous-flow reactor at 553 K and 101.3 kPa. Samples were sieved to retain particles with 0.35–0.42 mm diameter for catalytic measurements and pretreated in air at 773 K for 2 h before reaction. Phenol (P) and acetic acid (AA) were introduced (P/AA = 1) via a syringe pump and vaporized into flowing N_2 to give a $\text{N}_2/(\text{P} + \text{AA})$ ratio of 45. Standard catalytic tests were conducted at a contact time (W/F_p^0) of 146 g h/mol and gas-hour space velocity (GHSV) of 235 cm^3 STP/g min. The exit gases were analyzed on-line using an Hewlett-Packard 5890 chromatograph equipped with a Supelcowax 10TM column and a flame ionization detector. Data were collected every 25 min for about 6 h. Main products of phenol acylation with acetic acid were phenyl acetate (PA), *ortho*-hydroxyacetophenone and *para*-hydroxyacetophenone; *para*-acetoxyacetophenone (*p*-AXAP) was detected in trace amounts. Phenol conversion (X_p , mol of phenol reacted/mol of phenol fed) was calculated as: $X_p = \sum Y_i / (\sum Y_i + Y_p)$, where $\sum Y_i$ is the molar fraction of products formed from phenol and Y_p is the outlet molar fraction of phenol. The selectivity to product *i* (S_i , mol of

product i /mol of phenol reacted) was determined as: S_i (%) = $[Y_i/\sum Y_i]100$. Product yields (η_i , mol of product i /mol of phenol fed) were calculated as $\eta_i = S_i X_P$.

The gas-phase reactions of PA and o -HAP with AA were studied using the same reaction unit and chromatographic analysis than those described above for acylation of P with AA. The reaction conditions for PA with AA were: $T = 553$ K, $P = 101.3$ kPa, $P_{PA} = P_{AA} = 0.638$ kPa, $W/F_{PA}^0 = 43.1$ g h/mol; for o -HAP with AA: $T = 553$ K, $P = 101.3$ kPa, $P_{AA} = 1.8$ kPa, $P_{o-HAP} = 0.45$ kPa, $W/F_{o-HAP}^0 = 350$ g h/mol.

3. Results and discussion

3.1. Catalyst characterization

The physico-chemical characteristics (surface area, pore diameter and chemical composition) of the samples used in this work are summarized in Table 1. XRD patterns of Al-MCM-41 sample showed that this sample is well crystallized and exhibit a strong diffraction peak at 2.2° corresponding to (100) reflection, no other crystalline phases were observed. Sample acid properties were probed by TPD of NH_3 preadsorbed at 373 K. The obtained TPD curves are shown in Fig. 1. The NH_3 surface densities for acid sites were obtained by deconvolution and integration of TPD traces and are presented in Table 1. The evolved NH_3 from HY and HZSM-5 gave rise to a peak at 483–493 K and a broad band between 573 and 773 K. In contrast, HBeta and Al-MCM-41 samples did not exhibit the high-temperature NH_3 band but a single asymmetric broad band with a maximum around 482–496 K. On an areal basis, zeolites HY and HZSM-5 exhibited the highest surface acid density (about 2.2 mmol/m²), followed by HBeta (0.9 μ mol/m²) and Al-MCM-41 (0.4 μ mol/m²) samples.

The density and nature of surface acid sites were determined from the FTIR spectra of adsorbed pyridine. Fig. 2 compares the FTIR spectra obtained on samples HY, HZSM-5, HBeta and Al-MCM-41, after admission of pyridine, adsorption at room temperature and evacuation at 423 K. The FTIR spectra of Fig. 2 show well defined absorption peaks because physisorbed pyridine was eliminated after evacuation at 423 K. The pyridine absorption bands at around 1540 cm⁻¹ and between 1440 and 1460 cm⁻¹ arise from pyridine adsorbed on Brönsted and Lewis acid sites, respectively, on zeolites [20,21] and

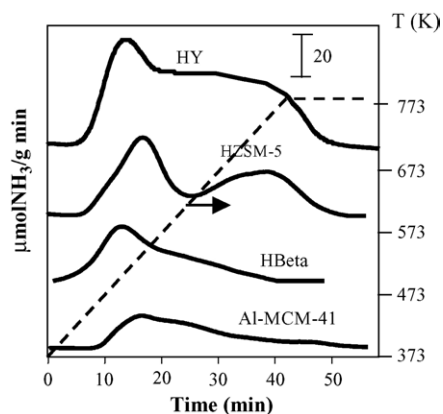


Fig. 1. TPD profiles of NH_3 on Al-MCM-41 and acid zeolites. Heating rate: 10 K/min.

Al-MCM-41 [22,23]. The relative contributions of Lewis and Brönsted acid sites were obtained then by deconvolution and integration of pyridine absorption bands appearing in Fig. 2 at around 1450 and 1540 cm⁻¹, respectively. Results are given in Table 1. In general, the band at 1540 cm⁻¹ characteristic for pyridinium ions does not change in wavenumber upon varying the sample acidity, but the frequency of the band accounting for coordinately bound pyridine increases with the strength of interaction. FTIR spectra of Fig. 2 show that on Al-MCM-41 the coordinately bound pyridine band appears at 1455 cm⁻¹, which reflects the adsorption of pyridine on Lewis acid sites associated with tricoordinate Al atoms. In agreement with the results obtained by TPD of NH_3 , the amount of pyridine adsorbed on Al-MCM-41 after evacuation at 423 K, in particular, on Brönsted sites, is clearly lower as compared to acid zeolites, reflecting the moderate acidic character of mesoporous Al-MCM-41 sample. The areal peak relationship between Lewis (L) and Brönsted (B) sites on Al-MCM-41 was $L/B = 4.2$, which is close to that reported for Al-MCM-41 samples containing similar Si/Al ratio [23]. The pyridine absorption bands associated with Brönsted and Lewis acid sites in Fig. 2 appears on zeolite HY at 1542 and 1454 cm⁻¹, respectively. These two bands were present even after evacuation of zeolite HY at 723 K, thereby, indicating that zeolite HY contains strong Brönsted and Lewis acid sites. The L/B ratio on HY was 1.5. On zeolite HZSM-5, the band of adsorbed pyridine on Lewis acid sites is splitted in two overlapping peaks at 1445 and 1455 cm⁻¹, respectively, in

Table 1

Physical properties, chemical composition and acidity characterization of the catalysts used in this work

Catalyst	Surface area, S_g (m ² /g)	Pore diameter, \bar{d}_p (Å)	Si/Al	TPD of NH_3		FTIR of pyridine	
				(μ mol/g)	(μ mol/m ²)	Brönsted sites (area/g)	Lewis sites (area/g)
HY	660	7.4	2.4	1380	2.1	310	465
HZSM-5	350	5.5	20	770	2.2	337	341
HBeta	560	6.7	25	500	0.9	150	151
Al-MCM-41	925	30	18	340	0.4	32	135

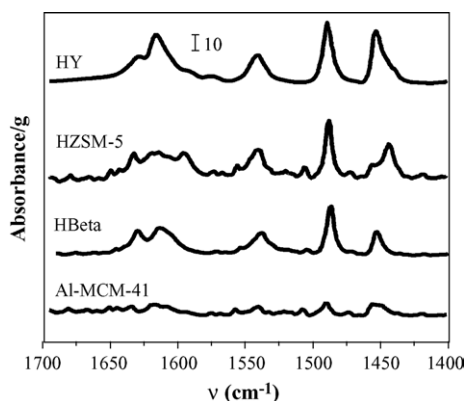


Fig. 2. FTIR spectra of pyridine adsorbed on Al-MCM-41 and acid zeolites at 298 K and evacuated at 423 K for 0.5 h.

agreement with previous reports [24]. It has been suggested that the Lewis acidity on protonic ZSM-5 is due to Al located in the zeolite framework, probably generated during calcination, resulting in partial hydrolysis of Al–O bonds [24]. Zeolite HZSM-5 contained a similar concentration of Brönsted and Lewis acid sites (Table 1). Finally, on HBeta, the pyridine adsorbed on Brönsted and Lewis acid sites appeared at 1542 and 1455 cm^{-1} , respectively. Consistent with the results obtained by TPD of NH_3 , the pyridine adsorption on HBeta confirmed that this zeolite is less acidic than zeolites HY and HZSM-5. The amount of pyridine adsorbed on both Lewis and Brönsted was, in fact, significantly lower than those adsorbed on HY and HZSM-5 samples. The L/B ratio on HBeta was close to one.

3.2. Catalytic results

Table 2 shows phenol conversion (X_P) and product selectivities (S_i) obtained for all the samples at times zero. Because of catalyst deactivation, values at time zero were obtained by extrapolating to zero the time-on-stream curves using semi-logarithmic plots. On all the samples, the initial formation of *o*-HAP was highly favored compared to that of *p*-HAP. Zeolites HZSM-5 and HY were the most active samples and exhibited the highest selectivities to *o*-HAP, but while formation of *p*-HAP was negligible on HZSM-5, the $S_{p\text{-HAP}}^0$ value was 8.9% on HY. On the other hand, the initial

Table 2
Catalytic and deactivation results for the acylation of phenol with acetic acid

Catalysts	Catalytic results at $t = 0$				Deactivation results	
	X_P^0	$S_{o\text{-HAP}}^0$	$S_{p\text{-HAP}}^0$	S_{PA}^0	$d_0 \times 10^{3a}$ (h^{-1})	C^b (%)
HY	15.0	69.1	8.9	22.0	7.8	18.4
HZSM-5	18.2	67.1	0.2	32.7	0.03	2.9
HBeta	12.7	65.1	4.6	30.3	4.5	9.3
Al-MCM-41	12.9	52.3	1.2	46.5	3.6	5.3

$T = 553 \text{ K}$, $W/F_P^0 = 146 \text{ g h/mol}$; $P/AA = 1$, $N_2/(P + AA) = 45$.

^a Initial deactivation, $d_0 = -(da/dt)_t = 0$.

^b Carbon formed after the 6 h runs.

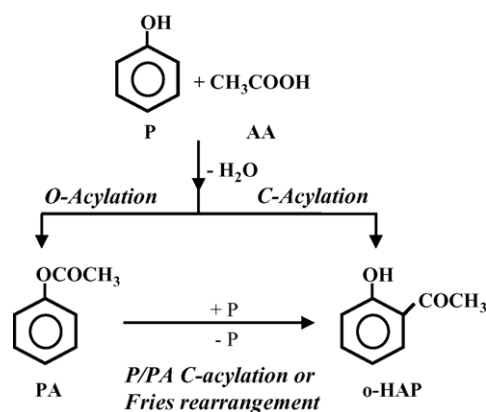


Fig. 3. Reaction network for the synthesis of *o*-HAP from phenol and acetic acid on solid acids [18].

conversion of phenol was similar on HBeta and Al-MCM-41 samples. However, formation of *o*-HAP was clearly lower on Al-MCM-41 ($S_{o\text{-HAP}}^0 = 52.3\%$) compared to that on HBeta ($S_{o\text{-HAP}}^0 = 65.1\%$).

In a previous paper [18], we studied the reaction mechanism of the gas-phase synthesis of hydroxyacetophenones on solid acids by acylation of P with AA. By determining the effect of contact time on the product distribution, we identified the primary and secondary reaction pathways involved in the synthesis of *o*-HAP from phenol and acetic acid. Specifically, we proposed (Fig. 3) that *o*-HAP is formed from phenol and AA via two parallel pathways: (i) the direct C-acylation of phenol and (ii) the O-acylation of phenol forming the PA intermediate which is consecutively transformed to *o*-HAP via intramolecular Fries rearrangement or intermolecular phenol/PA C-acylation. We observed [18] that the relative rate of the different pathways involved in Fig. 3 greatly depend on the solid acid employed. In particular, the *o*-HAP formation rate was higher on acid zeolites containing strong Brönsted and Lewis acid sites as compared to samples containing only Brönsted acid sites, such as heteropolyacid-based catalysts or exhibiting moderate acidity, such as silica–alumina. Similarly, results reported here in Table 1 show that strongly acid HY and HZSM-5 zeolites promote the *o*-HAP formation at higher rates as compared to HBeta or Al-MCM-41 samples that exhibit moderate acidity. This suggest that both strong Brönsted and Lewis sites are required to produce efficiently *o*-HAP via both the direct C-acylation of phenol and the acylation of phenyl acetate intermediate formed from O-acylation of phenol.

3.3. Deactivation results

On HY, HBeta and Al-MCM-41, the phenol conversion practically remained unmodified during the 6-h catalytic test but the *o*-HAP formation rate continuously decreased and as a consequence, the product selectivity significantly changed with time-on-stream. For example, on HY, the initial *o*-HAP selectivity (69.1%) dropped to 8.7% after 6 h of reaction;

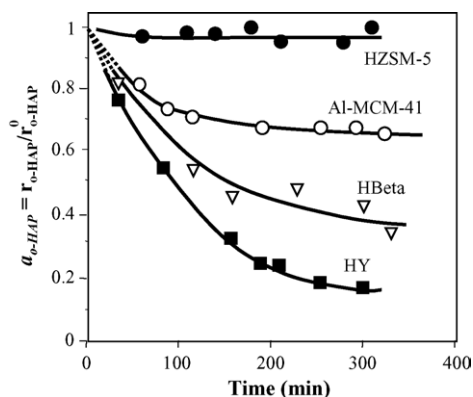


Fig. 4. Acylation of phenol with acetic acid. Activity for *o*-HAP formation ($a_{o\text{-HAP}}$) as a function of time [553 K, 101.3 kPa total pressure, $W/F_P^0 = 146$ g h/mol, $P/AA = 1$, $N_2/(P + AA) = 45$].

correspondingly, the PA selectivity increased from 22.0% at time zero to 90.3% at the end of the reaction. In contrast, on HZSM-5, not only the phenol conversion but also the product selectivities did not change with time-on-stream, i.e. we did not observe on HZSM-5 sample, any significant activity decay for the *o*-HAP formation rate during the catalytic run.

In Fig. 4, we have plotted the evolution of the activity for the formation of *o*-HAP ($a_{o\text{-HAP}}$) as a function of time-on-stream. The activity $a_{o\text{-HAP}}$ is defined as $a_{o\text{-HAP}} = r_{o\text{-HAP}}/r_{o\text{-HAP}}^0$, where $r_{o\text{-HAP}}$ and $r_{o\text{-HAP}}^0$ are the formation rates of *o*-HAP at times t and zero, respectively. Fig. 4 shows that $a_{o\text{-HAP}}$ does not change with time on HZSM-5, but rapidly decreases on the other samples, particularly, on sample HY. To quantify the *o*-HAP formation rate decay, we measured the initial catalyst deactivation, d_0 (h^{-1}) = $-(da_{o\text{-HAP}}/dt)_{t=0}$, as the initial slope of the activity versus time curves in Fig. 4. The resulting d_0 values are presented in Table 2. Coke formed on HZSM-5, Al-MCM-41, HY and HBeta was determined by analyzing the samples after the catalytic tests by temperature-programmed oxidation. The amount of carbon on the samples was measured from the area under the curves of % C versus T and the values ranged from 18.4% C on HY to 2.9% C on ZSM-5 (Table 2). The % C formed on Al-MCM-41, HBeta and HY increased with the sample acidity, i.e. % C was in the order Al-MCM-41 < HBeta < HY. On the other hand, by comparing the values of d_0 and % C in Table 2, it is observed that d_0 increases with the amount of carbon on the sample, thereby, suggesting that the activity decay for the formation of *o*-HAP is caused by coke formation.

3.4. Deactivation mechanism

In order to get more details on the deactivation mechanism of phenol acylation with acetic acid, we quantitatively evaluate the effect that varying space time W/F_P^0 (and consequently, X_P^0) has on *o*-HAP formation rate decay by determining the initial catalyst deactivation, d_0

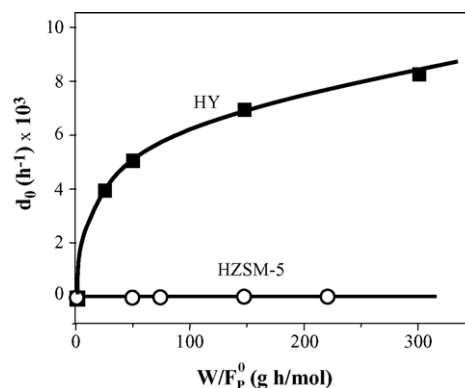


Fig. 5. Acylation of phenol with acetic acid. Initial deactivation of *o*-HAP formation rate, $d_0 = -(da_{o\text{-HAP}}/dt)_{t=0}$, as a function of contact time on HY and HZSM-5 samples [553 K, 101.3 kPa total pressure, $P/AA = 1$, $N_2/(P + AA) = 45$].

(h^{-1}) = $-(da_{o\text{-HAP}}/dt)_{t=0}$, as the initial slope of the activity versus time curves obtained for different W/F_P^0 values on HY and HZSM-5 samples. The obtained d_0 values are represented as a function of W/F_P^0 in Fig. 5. Zeolite HZSM-5 does not deactivate by increasing W/F_P^0 and X_P^0 up to 220 g h/mol and 25%, respectively, but on HY samples, d_0 increases with W/F_P^0 , thereby, suggesting that coke is formed via consecutive side reactions from the products of the reaction.

To obtain more insight on the species responsible for coke formation, we decided to investigate the activity decay and coke formation that take place when one or several intermediate compounds involved in the reaction network of Fig. 3 are contacted directly with the solid acids. We first studied the catalyst activity decay during the conversion of PA on HZSM-5 by employing different contact times. PA is the key intermediate to yield *o*-HAP from phenol by a consecutive two steps mechanism. In Fig. 6, we plotted the evolution of the activity for the conversion of PA, $a_{PA} = r_{PA}/r_{PA}^0$, as a function of time for different W/F_{PA}^0 values. Fig. 6 shows that a_{PA} clearly diminishes with time-on-stream on zeolite HZSM-5 when the reactant is PA. PA was converted to P, *o*-HAP and *p*-HAP, but formation of phenol was predominant, in particular, for higher contact times. The initial selectivity to *o*- and *p*-HAP isomers

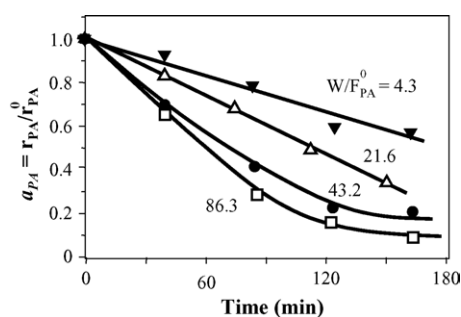


Fig. 6. Activity for phenyl acetate conversion (a_{PA}) as a function of time on HZSM-5 for different contact times [553 K, 101.3 kPa total pressure, $P_{PA} = 0.638$ kPa].

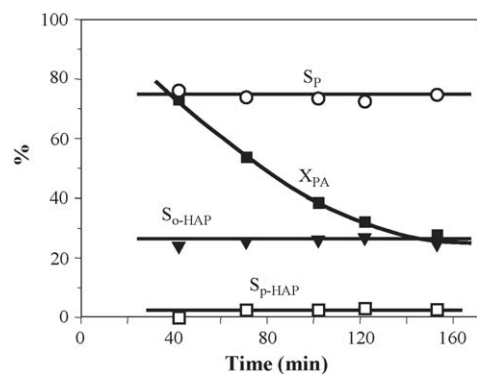
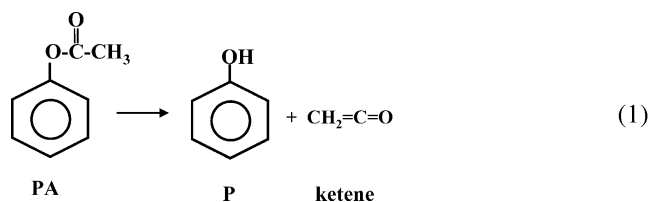


Fig. 7. Phenyl acetate/acetic acid reactions on HZSM-5. Selectivities (S_i) and phenyl acetate conversion (X_{PA}) as a function of time-on-stream [553 K, 101.3 kPa total pressure, $P_{PA} = P_{AA} = 0.638$ kPa, $W/F_P^0 = 43.1$ g h/mol].

reached, in fact, a value of about 28% for $W/F_{PA}^0 = 22$ g h/mol, but rapidly decreased then for higher W/F_{PA}^0 values and was negligible for $W/F_{PA}^0 = 86.3$ g h/mol and $X_{PA}^0 = 86\%$. Regarding catalyst deactivation, it is significant to note here that HZSM-5 rapidly deactivates when contacted directly with PA in contrast with the high stability that this zeolite showed for the *o*-HAP synthesis from phenol and AA (Fig. 4). To obtain further insight on the catalyst deactivation mechanism, an additional catalytic test was carried out on HZSM-5 by cofeeding PA with AA. In Fig. 7, we plotted the evolution of PA conversion and product selectivities as a function of time. It is observed that X_{PA}^0 decreases while the product selectivities remain constant with time-on-stream. The PA/AA reaction produced phenol ($S_P^0 = 73.8\%$), *o*-HAP ($S_{o\text{-HAP}}^0 = 25.5\%$) and minor amounts of *p*-HAP.

In summary, results from Figs. 6 and 7 show that HZSM-5 rapidly deactivates when PA or a P + PA mixture are used as reactants. This may be explained by considering that in the case that PA is added alone or in a PA + AA mixture, the conversion of PA to P occurs with simultaneous formation of ketenes.



Ketenes are extremely reactive and unstable compounds that dimerize to diketenes and polymerize very quickly [25]. As a matter of fact, the formation of coke via the irreversible polymerization of highly reactive ketene is the main reason of the rapid deactivation observed during the liquid-phase Fries rearrangement of PA on solid acids [7,26].

Taking into account these last results, the question is now why zeolite HZSM-5 does not deactivate during the acylation of phenol with AA in spite of forming significant amounts of PA (Fig. 4 and Table 2). A probable answer arises from the reaction network of Fig. 3, which shows that

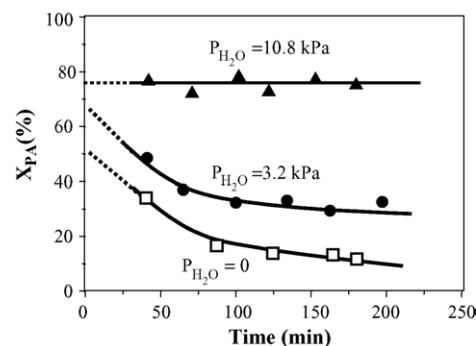
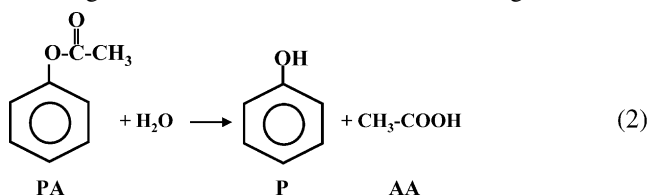


Fig. 8. Effect of water pressure on the phenyl acetate conversion (X_{PA}) on HZSM-5 [553 K, 101.3 kPa total pressure, $P_{PA} = 0.638$ kPa, $W/F_P^0 = 43.1$ g h/mol].

formation of PA from the acylation of P with AA occurs with the simultaneous formation of water. The presence of moisture may neutralize any consecutive formation of ketenes because water rapidly reacts with ketenes to produce acetic acid [27] and would, thereby, suppress the reaction pathway forming coke from ketene precursors. In order to verify this assumption, we carried out additional catalytic tests by cofeeding water and PA on HZSM-5. Results are given in Fig. 8, which shows the evolution of X_{PA} as a function of time-on-stream for different concentrations of water in the feed. In absence of water, X_{PA} rapidly dropped as a function of time, but the catalyst activity decay diminished by adding water to PA. For a value of $P_{H_2O}^0 = 10.8$ kPa, the PA conversion was almost constant over the entire catalytic test. The addition of water also increased the initial conversion of PA, X_{PA}^0 , thereby, indicating a positive order in water for PA/water conversion reactions. On the other hand, in absence of water, PA was converted exclusively to P ($S_P^0 \cong 94\%$) and *o*-HAP, but the addition of water caused the simultaneous formation of acetic acid. For a value of $P_{H_2O}^0 = 10.8$ kPa, we detected in the effluent a PA/AA molar ratio close to 0.9, thereby, showing that PA is converted via the following reaction.



These results clearly support, therefore, the assumption that in presence of water, PA is converted essentially via reaction 2. Formation of ketene according to reaction 1 will not take place to a significant extent, then, in presence of water. In other words, the activity decay observed during the acylation of P with AA on HY, HBeta and Al-MCM-41 samples (Fig. 4) is not caused for any coke formed from polymerization of ketene precursors because water is a primary product of the reaction and rapidly transforms ketene to acetic acid.

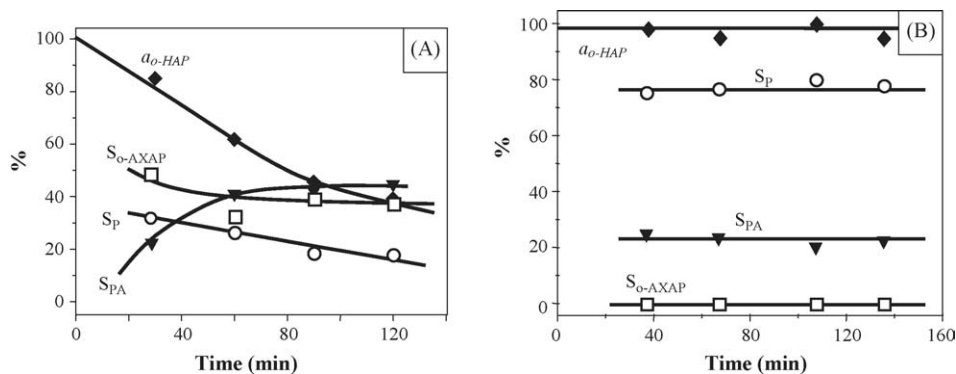
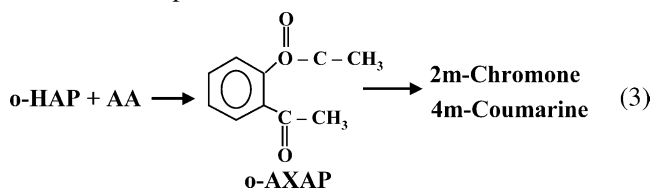


Fig. 9. *o*-HAP/acetic acid reactions. Activity for *o*-HAP conversion ($a'_{o\text{-HAP}}$) and product distribution on: (A) HY and (B) HZSM-5 [553 K, 101.3 kPa total pressure, $P_{\text{AA}} = 1.8$ kPa, $P_{o\text{-HAP}} = 0.45$ kPa, $W/F_{o\text{-HAP}}^0 = 350$ g h/mol].

Finally, in an attempt to ascertain the nature of the species responsible for coke formation in the synthesis of *o*-HAP from acylation of P with AA, we studied the conversion of *o*-HAP with AA on zeolites HY and ZSM-5. In Fig. 9, we plotted the evolution of the activity for *o*-HAP conversion ($a'_{o\text{-HAP}}$) and product selectivities as a function of time-on-stream. The coinjection of *o*-HAP with AA on HY formed P, PA and *o*-acetoxyacetophenone (*o*-AXAP) (Fig. 9A). Rapid activity decay was observed and after 120 min on stream the amount of carbon deposited was 19.0%. In contrast, HZSM-5 did not produce *o*-AXAP and did not deactivate during *o*-HAP/AA conversion reactions (Fig. 9B). After 150 min on stream, the amount of carbon formed on HZSM-5 was only 1.5%. The observed HY deactivation in Fig. 9A seems to be related, therefore, with the formation of *o*-AXAP. In a previous paper [28], it was reported that coke formed on MFI zeolites during the acylation of phenol with AA is mainly constituted by methylnaphtols, 2-methylchromone and 4-methylcoumarine. Formation of 2*m*-chromone and 4*m*-coumarine may take place from *o*-HAP and AA via the initial formation of *o*-AXAP as depicted in reaction 3.



The assumption that coke is formed essentially via reaction 3 is also consistent with results in Fig. 9B showing that zeolite HZSM-5 that does not produce *o*-AXAP when cofeeding *o*-HAP and AA, does not deactivate. It seems, therefore, that the superior stability of zeolite HZSM-5 is due to a shape-selectivity effect that avoids formation of the coke precursor specie. In other words, zeolite HZSM-5 does not deactivate because its narrow pore size structure hinders the formation of *o*-AXAP that is the key coke precursor in the gas-phase acylation of phenol with acetic acid.

4. Conclusions

The formation rate of *o*-hydroxyacetophenone from the gas-phase acylation of phenol with acetic acid on samples Al-MCM-41, HBeta and HY rapidly decreases on stream because of coke formation. The activity decay rate increases with the amount of carbon on the sample that, in turn, increases with increasing sample acidity. Coke precursors are not formed from ketene polymerization because water is a primary product of phenol conversion reactions and rapidly transforms ketene to acetic acid. The key intermediate compound for coke formation would be *o*-acetoxyacetophenone that is produced from reaction between *o*-hydroxyacetophenone and acetic acid and forms heavier compounds via condensation reactions. On zeolite HZSM-5, the *o*-hydroxyacetophenone yield remains stable on stream and formation of coke is drastically suppressed. The superior stability of zeolite HZSM-5 is explained by a shape-selectivity effect, by considering that the microporous structure of this zeolite avoids the formation of bulky *o*-acetoxyacetophenone.

Acknowledgements

We thank the Universidad Nacional del Litoral (UNL), Consejo Nacional de Investigaciones Científicas y Técnicas (CONICET) and Agencia Nacional de Promoción Científica y Tecnológica (ANPCyT), Argentina, for the financial support of this work. We are grateful to H. Cabral for IR spectroscopy measurements.

References

- [1] A. Commarieu, W. Hölderich, J.A. Laffitee, M. Dupont, J. Mol. Catal. A Chem. 182 (2002) 137.
- [2] I. Uwaydah, M. Aslam, C. Brown, S. Fitzhenry, J. McDonough, US Patent 5,696,274 (1997).
- [3] J. Fritch, O. Fruchey, T. Horlenko, Hoechst Celanese Corporation, US Patent 4,954,652, (1990).

- [4] A. Vogt, H. Kouwenhoven, R. Prins, *Appl. Catal.* 123 (1995) 37.
- [5] F. Jayat, M.J. Sabater Picot, M. Guisnet, *Catal. Lett.* 41 (1996) 181.
- [6] E.F. Kozhevnikova, J. Quartararo, I.V. Kozhevnikov, *Appl. Catal. A Gen.* 245 (2003) 69.
- [7] E. Heitling, F. Roessner, E. van Steen, *J. Mol. Catal. A Chem.* 216 (2004) 61.
- [8] V. Pouilloux, J.-P. Bodibo, I. Neves, M. Gubelnann, G. Perot, M. Guisnet, in: M. Guisnet, et al. (Eds.), *Heterogeneous Catalysis and Fine Chemicals II*, Elsevier, Amsterdam, 1991, p. p. 513.
- [9] V. Borzatta, G. Busca, E. Poluzzi, V. Roseetti, M. Trombetta, A. Vaccari, *Appl. Catal. A Gen.* 257 (2004) 85.
- [10] J. Mueller, W. Wiersdorff, W. Kirschenlohr, G. Schwantje, US Patent 4,508,924, BASF (1985).
- [11] G.N. Mott, Celanese Corporation, US Patent 4,607,125, 1986.
- [12] U. Freese, F. Hinrich, F. Roessner, *Catal. Today* 49 (1999) 237.
- [13] M. Guisnet, D.B. Lukyanov, F. Jayat, P. Magnoux, I. Neves, *Ind. Eng. Chem. Res.* 34 (1995) 1624.
- [14] K.G. Bhattacharyya, A.K. Talukdar, P. Das, S. Sivasanker, *Catal. Commun.* 2 (2001) 105.
- [15] F. Jayat, M. Guisnet, M. Goldwasser, G. Giannetto, *Stud. Surf. Sci. Catal.* 105 (1997) 1149.
- [16] Y.V. Subba Rao, S.J. Kulkarni, M. Subrahmanyam, A.V. Rama Rao, *Appl. Catal. A Gen.* 133 (1995) 1.
- [17] D. Rohan, C. Canaff, P. Magnoux, M. Guisnet, *J. Molec. Catal. A Chem.* 129 (1998) 69.
- [18] C.L. Padró, C.R. Apesteguía, *J. Catal.* 226 (2004) 308.
- [19] K.J. Edler, J.W. White, *Chem. Mater.* 9 (1997) 1226.
- [20] E.P. Parry, *J. Catal.* 2 (1963) 371.
- [21] J.W. Ward, *J. Catal.* 10 (1968) 34.
- [22] J. Wang, L. Huang, H. Chen, Q. Li, *Catal. Lett.* 55 (1998) 157.
- [23] A. Sakthivel, S.E. Dapurkar, N.M. Gupta, S.K. Kulshreshtha, P. Selvam, *Microporous Mesoporous Mater.* 65 (2003) 177.
- [24] G.I. Woolery, G.H. Kuehl, H.C. Timken, A.W. Chester, J.C. Vartuli, *Zeolites* 19 (1997) 288.
- [25] T.T. Tidwell, *Acc. Chem. Res.* 23 (1990) 273.
- [26] A. Heidekum, M.A. Harmer, W.F. Hölderich, *J. Catal.* 176 (1998) 260.
- [27] E. Bothe, A.M. Dessouki, D. Schulte-Frohlinde, *J. Phys. Chem.* 84 (1980) 3270.
- [28] I. Neves, F. Jayat, P. Magnoux, G. Perot, F.R. Ribeiro, M. Gubelman, M. Guisnet, *J. Mol. Catal.* 93 (1994) 169.